Polymer Chemistry

ROYAL SOCIETY OF CHEMISTRY

PAPER

View Article Online
View Journal | View Issue

Check for updates

Cite this: *Polym. Chem.*, 2024, **15**, 4982

Long afterglow epoxidized soybean oil polymer composites with reversible dynamic cross-linking for intelligent coating†

Jiaman Hu,[a] Zihao Wang,[a] Minglin Yang,[a] Chuansong Yu,[a] Siyu Li,[a] Yinggang Miao,[b,c,d] Xiangqian Quan,[e,f] Jize Liu*[a] and Shiyang Shao *[a]

High-performance coatings with advanced functions such as long afterglow luminescence and self-healing have attracted great interest around the world, but the integration of these desirable multiple functions into a single composite system still remains a great challenge. Herein, an intelligent coating based on epoxidized soybean oil and modified long afterglow powders is presented for a self-healing intelligent coating. By constructing a dynamic hydrogen bonding network between natural polyphenols and epoxidized soybean oil, the obtained composites show desirable adhesive performances and self-healing ability: the shear strength of the obtained coating is able to reach 313.96 kPa while the self-healing efficiency was about 81.29% after a damage–healing process. Moreover, the introduction of SiO_2-modified $SrAl_2O_4$:Eu^{2+},Dy^{3+} powders endows the intelligent coating with long afterglow ability, which greatly benefits the visualized monitoring of small cracks. Meanwhile, the obtained bio-sourced composites could be degraded under anaerobic composting conditions within 5 days, and after degradation the long afterglow powders could be separated and recycled with almost consistent performance (luminescent intensity remains 95.19%) in contrast to the original powders. This study offers valuable examples and new insights for the high-value utilization of bio-based materials.

Received 2nd August 2024,
Accepted 28th October 2024

DOI: 10.1039/d4py00857j

rsc.li/polymers

Published on 02 noviembre 2024. Downloaded on 05/02/2026 6:04:43.

Introduction

A coating on the surface of metal and polymer materials is a key method to effectively protect the material from corrosion and damage.[1,2] When the coating layer is in excellent condition, it offers excellent physical shielding against a corrosive medium, protecting the substrate from corrosion and damage.[3–5] Most existing synthetic coatings are formulated with petrochemical resins, but their weak adhesion to metals and polymer material, inevitable interfacial debonding and micro-crack propagation significantly affect their shielding protection ability, as the development of electrochemical corrosion and microscopic damage may cause an overall process of domino-like corrosion damage.[6–9] In addition, petroleum-based coatings, due to their non-biodegradable nature, may lead to further microplastic pollution after being damaged.[10–13] Therefore, high-performance, advanced-functionality and environmentally-friendly matrices are one of the most important development trends in next-generation coatings, and as a result high-adhesion, self-healing and biodegradable smart coatings have attracted extensive attention from researchers worldwide.[14,15]

Bio-based and bio-degradable materials are gradually becoming another new leading industry driving scientific and technological innovation and economic development in the contemporary world due to their green, environmentally friendly, and low-carbon characteristics.[16,17] An elaborate multi-scale structural design to endow bio-based materials with the desired comprehensive performance which can match or even exceed that of petroleum-based coatings is a highly attractive topic, but it remains a formidable challenge.[15,18,19] For example, Yang *et al.* isolated water-insoluble lignin from biomass and obtained a simple bio-based wood adhesive. Through the self-cross-linking of lignin during the hot-press-

[a]*School of Materials Science and Engineering, Hainan University, Haikou, 570228 Hainan, China. E-mail: ljz@hainanu.edu.cn, ssyang@hainanu.edu.cn*
[b]*Shaanxi Key Laboratory of Impact Dynamics and its Engineering Application, School of Aeronautics, Northwestern Polytechnical University, Xi'an 710072, China*
[c]*Joint International Research Laboratory of Impact Dynamics and its Engineering Applications, School of Aeronautics, Northwestern Polytechnical University, Xi'an 710072, China*
[d]*National Key Laboratory of Strength and Structural Integrity, Xi'an 710072, China*
[e]*Institute of Deep-Sea Science and Engineering, Chinese Academy of Sciences, Sanya 572000, China*
[f]*Department of Mechanical and Aerospace Engineering and Scripps Institution of Oceanography, University of California San Diego, La Jolla, CA 92093, USA*
†Electronic supplementary information (ESI) available. See DOI: https://doi.org/10.1039/d4py00857j

This journal is © The Royal Society of Chemistry 2024

Published on 02 noviembre 2024. Downloaded on 05/02/2026 6:04:43.

ing process, a high-performance wood adhesive was achieved after 100 °C for 2 min, and the adhesive strength could reach the Chinese National Standard GB/T 9846-2015.[20] Sun *et al.* prepared a novel bio-based supramolecular adhesive based on castor oil, melevodopa and Fe^{3+} ions. Owing to the strong coordination interaction between melevodopa-functionalized castor oil and Fe^{3+} ions, as well as the catechol units of melevodopa, the obtained adhesives achieved adhesion strengths of 14.6 MPa at room temperature and 9.5 MPa at −196 °C, which is the highest value reported for bio-based adhesives and supramolecular adhesives.[21] Among widely used bio-sourced polymer materials, epoxy soybean oil is an ideal candidate for the development of commercially viable environmentally friendly bio-based coatings because of its characteristics of inexpensiveness and readily availability.[22,23] However, the low cohesion energy and weak reactivity of non-polar epoxy soybean oil have always led to unsatisfactory adhesion and mechanical properties. Until now, how to design environmentally friendly cross-linking systems for high-performance epoxy soybean oil-based coating applications is still a crucial research direction.[24,25]

Optical signals account for 70% of the information received by humans, so the construction of luminous behaviour offers new opportunities for intelligent applications of organic coatings.[26] Long afterglow materials, which are able to store the acquired light energy and release it in the form of light continuously and slowly after removing the external light source, have attracted increasing attention for advanced applications in emergency lighting, traffic signs, interior decoration, display, anti-forgery and other fields.[27–29] For example, Liu *et al.* designed a novel near-infrared-persistent luminescence material $(Sr,Ba)(Ga,In)_{12}O_{19}:Cr^{3+}$ with efficient ultraviolet (UV)–red light charging capacity. After mixing with acrylic acid the obtained afterglow coating could be applied to metal for infrared tagging, for which the image can last more than 12 hours in the dark.[30] Zhou *et al.* prepared hour-scale ultralong afterglow polymer films by a molecular doping strategy. The afterglow of transparent and flexible polymer films can last for 11 h in air at room temperature and can be used for efficient flexible display, including information writing and erasure.[31] As a typical afterglow material, $SrAl_2O_4:Eu^{2+},Dy^{3+}$ possesses advantages including long and strong visible afterglow, which is able to endow the composite coatings with battery-free illumination during the night and is expected to increase the added value of the coatings.[28] However, the widely used $SrAl_2O_4:Eu^{2+},Dy^{3+}$ powder undergoes hydrolysis in contact with water, which may lead to serious degradation of the polymer matrix and limit its application.[32]

As mentioned above, the propagation of micro-cracks and the infiltration of small molecules (like water, oxygen, and ions) can accelerate metal corrosion through the electrochemical process, so early warning and spontaneous repair of micro-cracks are of crucial significance.[33–35] By introducing modified long afterglow $SrAl_2O_4:Eu^{2+},Dy^{3+}$ powder, the luminescence intensity and distribution of the obtained coatings will change under stress and defect conditions, which is expected to be applied to the non-contact and dynamically visualized monitoring of stress concentration and small cracks, and a warning technique can be achieved through the development of new analysis and identification technologies.[36–38] In addition, the design with multiple hydrogen bonds endows the coating with self-healing ability to repair small cracks, which could be able to significantly delay the corrosion process of metals and damage problems of polymer materials, providing a feasible strategy for the realization of green and long-life intelligent coatings.[39]

Herein, this paper presents an environmentally friendly, recyclable, long afterglow smart coating using natural bio-based materials and long afterglow materials for self-healing intelligent coatings. Epoxidized soybean oil (Soy) was first cured with malic acid (Mal) and tannic acid (Ta), and the obtained Soy-Mal-Ta (SMT) bio-sourced polymer with a large number of hydrogen bonds and polyphenol hydroxyl groups for the metal-polyphenol network (MPN) endows the coating with strong adhesion, and the ability to repair small cracks after damage. By incorporating $SrAl_2O_4:Eu^{2+},Dy^{3+}$ powder modified with a silane coupling agent containing epoxy groups, the long afterglow powders were composited with the bio-sourced matrix through strong covalent–noncovalent interfacial cross-linking, which greatly benefits the achievement of a visualized warning system for capturing the crack situation. Furthermore, the bio-sourced matrix could be bio-degraded in the soil while the modified powders could be reused through a simple density sorting process, which better conforms to the trend of a low-carbon future. This strategy is designed to meet the demand for advanced functional coatings with high adhesion, flexibility and damage warning functions for the prevention of steel cracking, which offers important examples and ideas for the high-value utilization of bio-based materials.

Experimental

Materials

Tannic acid (>96.0%) was purchased from Jiangsu Aikang Biomedical R&D Co., Ltd (China). Malic acid (98.0%) was purchased from Shanghai Boka Chemical Technology Co., Ltd (China). Epoxy soybean oil (ESO, 95.0%) was purchased from Guangzhou Suixin Chemical Co., Ltd (China). $SrAl_2O_4:Eu^{2+},Dy^{3+}$ powder was purchased from Chuangrong Chemical Technology Co., Ltd (China). Anhydrous ethanol (AR, >99.7%) was purchased from Shanghai Titan Technology Co., Ltd (China). Hydrochloric acid (HCl, AR) and sodium chloride (NaCl, AR, >99.5%) were purchased from Xilong Science Co., Ltd (China). 3-(Glycidoxypropyl)triethoxysilane (GC, >96.0%) was purchased from Shanghai Aladdin Biochemical Technology Co., Ltd (China). Urea (AR, 99.0%), tetraethyl orthosilicate (TEOS, GC, 99.0%) and ammonium bicarbonate (AR) were purchased from Shanghai Yien Chemical Technology Co., Ltd (China). All the reagents were used as received without further purification. The water used in all

Published on 02 noviembre 2024. Downloaded on 05/02/2026 6:04:43.

experiments was deionized and ultrafiltered to 18.2 MΩ·cm with an Ulupure ultrapure water system (China).

Preparation of modified $SrAl_2O_4:Eu^{2+},Dy^{3+}$ powder

First, 0.40 mL of TEOS was dissolved in a 200 mL mixture of distilled water and ethanol (volume ratio 1 : 1). Then a suitable amount of hydrochloric acid was added to adjust the pH value to 1, and it was kept under these conditions for 30 min until the solution was clarified and transparent. Then, ammonium bicarbonate was added to set the pH value to 6. After stirring for 5 min and increasing the temperature to 65 °C, 15 g of urea and 15 g of $SrAl_2O_4:Eu^{2+},Dy^{3+}$ powder were added to the solution; the continuous addition of urea brought the pH to about 10 and it was kept under stirring for 2 h. After that, the suspension was kept at room temperature for 1 h; then the powder was separated by filtration and washed with deionized water. Finally, the obtained SiO_2-modified powder was dried in an oven at 90 °C for 2 h. A mixture of dried modified SiO_2 powder and 3-(glycidoxypropyl)triethoxysilane solution (volume ratio 1 : 0.2) was added to 100 mL of distilled water. After stirring for 10 min and increasing the temperature to 65 °C, it was kept under stirring for 2 h. Then the powder was separated by filtration and washed with deionized water. Finally, the powder was dried in an oven at 90 °C for 2 h.

Preparation of modified $SrAl_2O_4:Eu^{2+},Dy^{3+}$ SMT coatings

One gram of epoxy soybean oil was added to a round-bottomed flask and heated to 70 °C in an oil bath. After sufficiently heating to decrease viscosity, 1 mL of a 0.5 g mL^{-1} tannic acid/ethyl alcohol solution was added to the epoxy soybean oil and mixed for about 5 min. Next, 0.4 g of malic acid was slowly added to the solution until completely dissolved. The reactants were heated overnight, removed from the oil bath and cooled to room temperature. The reactant was poured into a disposable Petri dish, the modified $SrAl_2O_4:Eu^{2+},Dy^{3+}$ was added, and the SMT coating was obtained by mixing it evenly with glass rods.

Lap shear tests

Lap shear tests were conducted on SMT-coating-adhered substrates using a WDW-1 microcomputer-controlled electronic universal testing machine from Jinan East Testing Machine Co., Ltd, China, with a testing speed of 500 mm min^{-1} and a substrate overlap area of 12.0 × 20.0 mm^2. Lap shear strength (or adhesive strength) is defined as the maximum debonding force obtained through lap shear tests divided by the overlapping area of adhesive.

Electrochemical impedance spectroscopy (EIS) tests

The anticorrosion performance of the SMT-coated steel was studied in 3.0 wt% NaCl solution through EIS analysis using an electrochemical station (CHI660E, Shanghai Chenhua). The frequency ranges were 10^5 to 10^{-1} Hz. The EIS measurements were performed on 3 cm^2 sections of pure uncoated carbon steel samples and carbon steel samples coated with SMT coatings in a three-electrode cell including a saturated calomel electrode (SCE) as reference electrode, a platinum rod as counter electrode, and a coated/steel sample as a working electrode.

SMT coating degradation and $SrAl_2O_4:Eu^{2+},Dy^{3+}$ powder recycle test

Paint degradation experiments were performed at room temperature. The above coating (2 g) was buried under wet bamboo powder for about 2 cm. The degradation of the coating was observed by removing the bamboo powder every other day, and the degraded coating was irradiated with a UV torch (365 nm, 8 W), and the images were captured and saved by a camera. After the coating was completely degraded, the mixture of powder and bamboo powder was removed and added to 250 mL of deionized water, followed by the addition of an appropriate amount of cellulase. After continuous stirring for 5 min, the temperature was increased to 65 °C and stirred continuously stirring for 3 to 5 h. The powder was filtered, separated and then dried in an oven at 80 °C.

SMT coating self-healing process

The process of crack self-healing was observed with an electron optical microscope (Lingling Star 4800-B Guangzhou Xinlun Technology Co., Ltd). The coating was evenly coated on the steel sheet, scratches were generated on the surface of the coating using a surgical blade (to simulate the generation of cracks), and the SMT coating was placed under an electron microscope, images were captured by a CCD camera, and video was recorded.

Ultraviolet (UV) resistance test of SMT coatings

An ultraviolet (UV) dark box (length, width and height: 265, 185, 95 mm) was made of an iron box and a UV lamp (6 W). The sample was placed in the middle of the box and a UV lamp was placed (5 cm) directly above it. The effective irradiation area was 117.75 × 10^{-4} m^2, when the irradiation intensity of the UV lamp was 509.55 W m^{-2}. The cumulative exposure times were 36 h, 72 h, 108 h, 144 h, and 180 h, respectively, for the UV-36 h, UV-72 h, UV-108 h, UV-144 h, and UV-180 h SMT coatings. By measuring the surface temperature of the sample (28 °C) (Fig. S1†), the temperature was found to increase only slightly.

Scanning electron microscopy (SEM)

The microscopic morphology of the experimental samples was observed with a JSM-6710F SEM (Hitachi, Japan) at an accelerating voltage of 10 kV. Prior to SEM observation, the samples were sprayed with gold (10 mA, 50 s).

Fourier transform infrared (FTIR) spectroscopy

FTIR analysis was undertaken with an FTIR spectrometer (model Frontier Dual Ranger, PerkinElmer, Waltham, MA, USA) in attenuated total reflectance (ATR) mode from 400 to 4000 cm^{-1} at room temperature, at 4 cm^{-1} resolution with 32 scans. FTIR data was then normalized and analysed using OriginPro 2021.

This journal is © The Royal Society of Chemistry 2024

Published on 02 noviembre 2024. Downloaded on 05/02/2026 6:04:43.

Laser confocal microscopy Raman spectroscopy

Laser confocal microscopy Raman spectroscopy (HORIBA, HR Evolution, France) with a 532 nm laser line was performed to characterize the spatial distribution of the different components.

Afterglow attenuation test

The time-resolved contour photoluminescence (PL) maps of SMT coatings were collected on an FLS-1000 spectrofluorometer (Britain, Edinburgh Instrument) equipped with an Xe lamp as the excitation source, with excitation time of 1200 s, and collection time of 5800 s.

Results and discussion

Design principle and preparation

Most existing coatings are based on petroleum-based chemical engineering products, and the inevitably occurring cracks during service life may lead to serious metal corrosion and microplastic pollution. It is of great significance to develop green, bio-sourced, and bio-degradable coatings with advanced functions like self-healing and crack monitoring. However, the repair of tiny cracks and visualized monitoring still remain a challenge. In this study, bio-based materials enriched with multiple reversible hydrogen bonds combined with long afterglow materials were designed for intelligent coating. As shown in Fig. 1, a bio-sourced intelligent coating was designed, made from epoxidized soybean oil, malic acid, and tannic acid (Fig. 1a). The epoxidized soybean oil (Soy) was cured by malic acid (Mal), and tannic acid (Ta), endowing the obtained Soy-Mal-Ta (SMT) bio-sourced polymer with a dynamic cross-linked network (Fig. 1b). The cross-linking network involved covalent bonding (an epoxy-ring opening reaction with the carboxyl group of malic acid) and noncovalent bonding (hydrogen bonding between phenolic hydroxyl groups of Ta and carboxyl groups of malic acid). Such a covalent–noncovalent cross-linking network, could significantly benefit the mechanical properties and is expected to endow the materials with recycling, reprocessing, and self-healing abilities.[40,41] Moreover, long afterglow $SrAl_2O_4$:Eu^{2+},Dy^{3+} powders were modified to increase the compatibility of the powder in functional coatings. By utilizing the luminescent properties of $SrAl_2O_4$:Eu^{2+}, Dy^{3+} powders, a crack visualization and early warning system

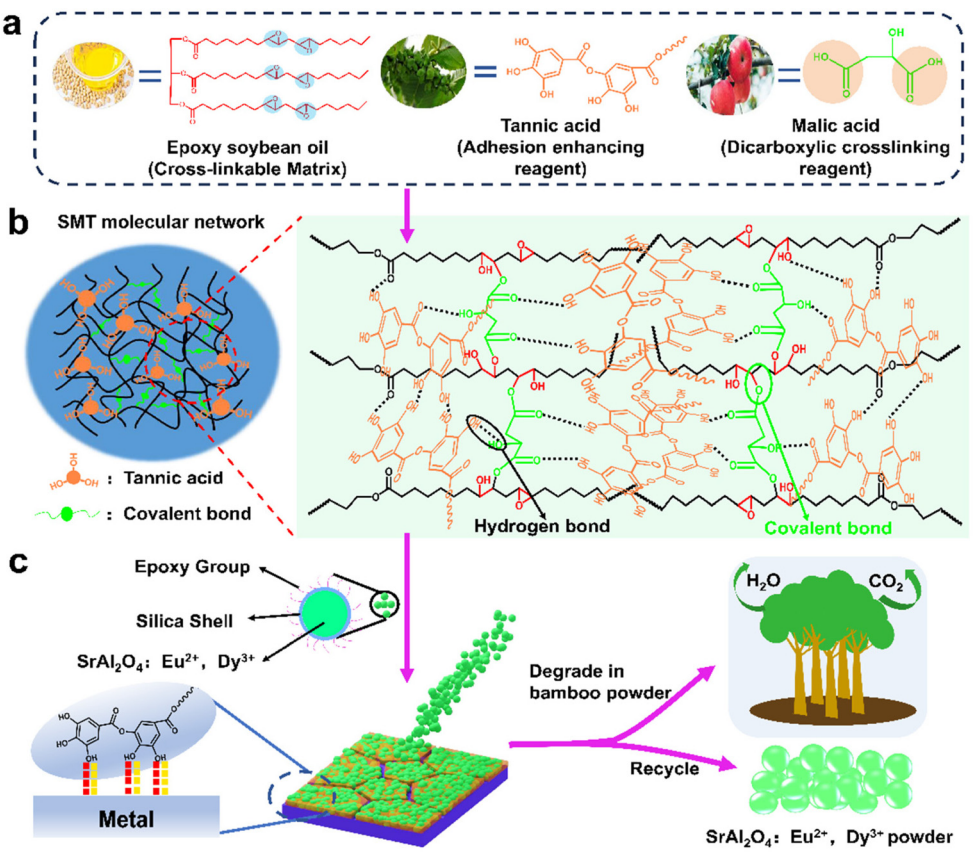

Fig. 1 (a) Soy-Mal-Ta (SMT) products are obtained by the reaction of bio-sourced epoxy soybean oil (Soy), tannic acid (Ta), and malic acid (Mal); the molecular structure formulas of the reactants are shown. (b) Molecular network of Soy binding to Mal and Ta in SMT products, and rich non-covalent interactions involving hydrogen bonds and phenolic hydroxyl groups. (c) The modified $SrAl_2O_4$:Eu^{2+},Dy^{3+} powders are simply mixed into the SMT product; the SMT coating is applied to the substrate, where the metal matrix interacts with the polyphenol; the coating is degraded and the powder recycled.

Published on 02 noviembre 2024. Downloaded on 05/02/2026 6:04:43.

can be enabled. At the same time, the system is rich in a variety of reversible hydrogen bonds and coordinate interaction between tannic acid and metal substrate (Fig. 1c), so that the crack could be able to heal in a short time.[42,43] Obviously, this study uses natural bio-sourced materials as raw materials, which is in line with the concepts of sustainable development and environmental protection. At the same time, these materials are biodegradable, and the $SrAl_2O_4$:Eu^{2+},Dy^{3+} powder can be recycled after degradation of the coating (Fig. 1c). The design of high-performance, multi-functional composite long afterglow coatings with reversible dynamic cross-linked networks can provide valuable advice for early warning of coating cracks and for sustainable materials.

Characterization of SMT coating structure and mechanical properties

According to the reported literature, $SrAl_2O_4$:Eu^{2+},Dy^{3+} powders undergo hydrolysis in contact with water, and the pH value increases significantly, which greatly limits their application in functional coatings.[44] As shown in Fig. 2a, in order to prepare SMT composite coatings, the SiO_2 protective layer was successfully constructed and epoxy groups were grafted onto the surface of the protective layer to prevent the hydrolysis of $SrAl_2O_4$:Eu^{2+},Dy^{3+}, and facilitate better compatibility with the SMT coating. In Fig. 2b, compared with unprocessed $SrAl_2O_4$:Eu^{2+},Dy^{3+} powder, the silica-modified $SrAl_2O_4$:Eu^{2+},Dy^{3+} powder exhibits an obvious peak at around 1098 cm^{-1}, which is ascribed to Si–O bonding. At the same time, there is a clear peak near 958 cm^{-1}, which is attributed to the epoxy group in the modified $SrAl_2O_4$:Eu^{2+},Dy^{3+} powder. These results indicate that the SiO_2 layer has been successfully constructed. Due to the presence of the silica layer, the obtained powder can be dispersed in water without hydrolysis, and the pH of the modified powder suspension is about 7, while the pH of the unmodified $SrAl_2O_4$:Eu^{2+},Dy^{3+} powder suspension is almost 8–9 after being dispersed in water for 1 h (Fig. S2†). In order to explore the influence of the SiO_2 protective layer on the PL intensity of the powder, comparative analysis shows that the $SrAl_2O_4$:Eu^{2+},Dy^{3+} powder with the SiO_2 protective layer exhibits a higher attenuation degree than the unmodified powder after the excitation source is removed (Fig. S3†).

The chemical structure of the SMT coatings was analysed by Fourier transform infrared spectroscopy (FTIR). In Fig. 2d, for the epoxy soybean oil, a peak at 950 cm^{-1} can be observed that correlates with the presence of epoxy groups.[45] In the FTIR spectrum of the product, termed SMT, the stretching vibration peaks of ester group –C═O and C–O–C were observed at 1738 cm^{-1} and 1090 cm^{-1}, respectively. The characteristic peak at 3165 cm^{-1} is attributed to hydrogen bond interaction between the phenolic hydroxyl group and the carboxylic acid group.[46,47] Furthermore, the intensity of the C═O characteristic peak of malic acid decreases and the characteristic peak for O–H disappears. These changes can be attributed to the reaction between the epoxy group in Soy and –COOH in malic acid.[22,48] The reaction temperature between the phenolic hydroxyl group of tannic acid and the epoxy group was above 200 °C under the catalytic conditions.[49] In this study, it reacted slowly but also participated in the cross-linking reaction of the whole system. SMT is an extensively cross-linked matrix and all three components are involved in covalent bond formation and the system is characterized by a large number of hydrogen bonding interactions.[50]

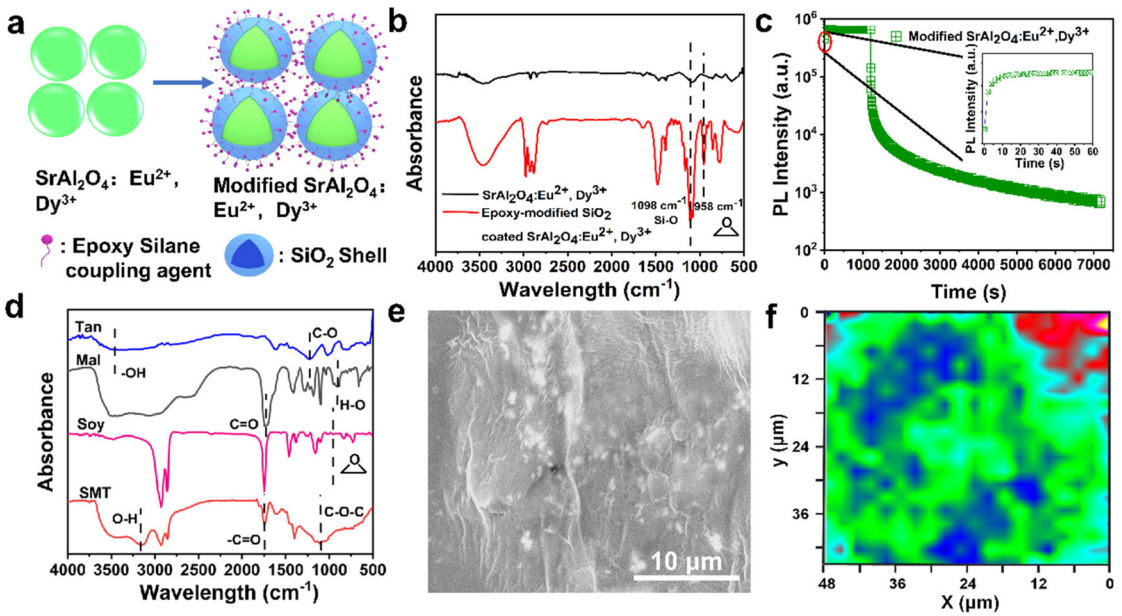

Fig. 2 (a) Schematic diagram of $SrAl_2O_4$:Eu^{2+},Dy^{3+} powder modification. (b) Comparison of FTIR spectra before and after $SrAl_2O_4$:Eu^{2+},Dy^{3+} powder modification. (c) Afterglow attenuation curve of the modified $SrAl_2O_4$:Eu^{2+},Dy^{3+} powder. (d) FTIR spectra of Tan, Mal, Soy, and the SMT product. (e) The SEM images of fracture surfaces for the SMT coating. (f) 2D Raman intensity mapping of the obtained SMT coating.

 This journal is © The Royal Society of Chemistry 2024

Published on 02 noviembre 2024. Downloaded on 05/02/2026 6:04:43.

In Fig. 2e, the SEM image can be observed in white for the modified $SrAl_2O_4$:Eu^{2+},Dy^{3+} powder with an average particle size of 0.5 μm. When cracks occur under stress, and the luminance at the crack area differs from other regions, it may be used for early warning. In Fig. 2f, laser confocal Raman microspectroscopy with a near-infrared (532 nm) laser and 3D Raman mapping was used to demonstrate the spatial distribution of the different components. Peaks around 2514 cm^{-1} (yellow-shaded region) belong to the characteristic region of modified $SrAl_2O_4$:Eu^{2+},Dy^{3+} powders (Fig. S4†), and the green to blue areas reveal the spatial distribution of the selected powders. The powder has been successfully loaded into the SMT polymer to form an SMT composite coating.

In order to evaluate the applicability and bond strength between the coating and substrate of SMT coatings, lap shear tests were performed on bonded sheets made of different materials using SMT coatings. In Fig. 3a, it can achieve bonding functions for different materials (such as glass, PP, PVC, PS, or PTFE). Fig. 3b illustrates a shear experiment in which the material is subjected to forces parallel to the coating. As shown in Fig. 3c and d, SMT coatings can be tightly bonded to various materials, and the bonding strengths of PTFE, Fe, PET, PI, PVC, and PC are 99.33, 164.70, 219.30, 221.83, 297.46, and 313.96 kPa, respectively. The SMT coating is able to not only achieve adhesion to metal but also shows ideal adhesion ability to polymer materials. The wide applicability of SMT coatings is due to the fact that catechol units can interact with different materials through hydrogen bonding, metal–ligand coordination, hydrophobic effects, *etc.*[51] As shown in Fig. 3e and f, a shear test was carried out using PC material at different tensile speeds. When the tensile speeds were 500, 100, 50, 10, 1, and 0.1 mm min^{-1}, the shear strengths of PC were 313.96, 110.33, 40.62, 25.45, 9.18, and 1.18 kPa, respectively. It can be concluded that as the tensile speed increases, the bond strength becomes larger, and the PC material exhibits strain rate dependence. As shown in Fig. 3g, the shear toughness at different tensile velocities is obtained by further calculating the stress–strain curves of the shear

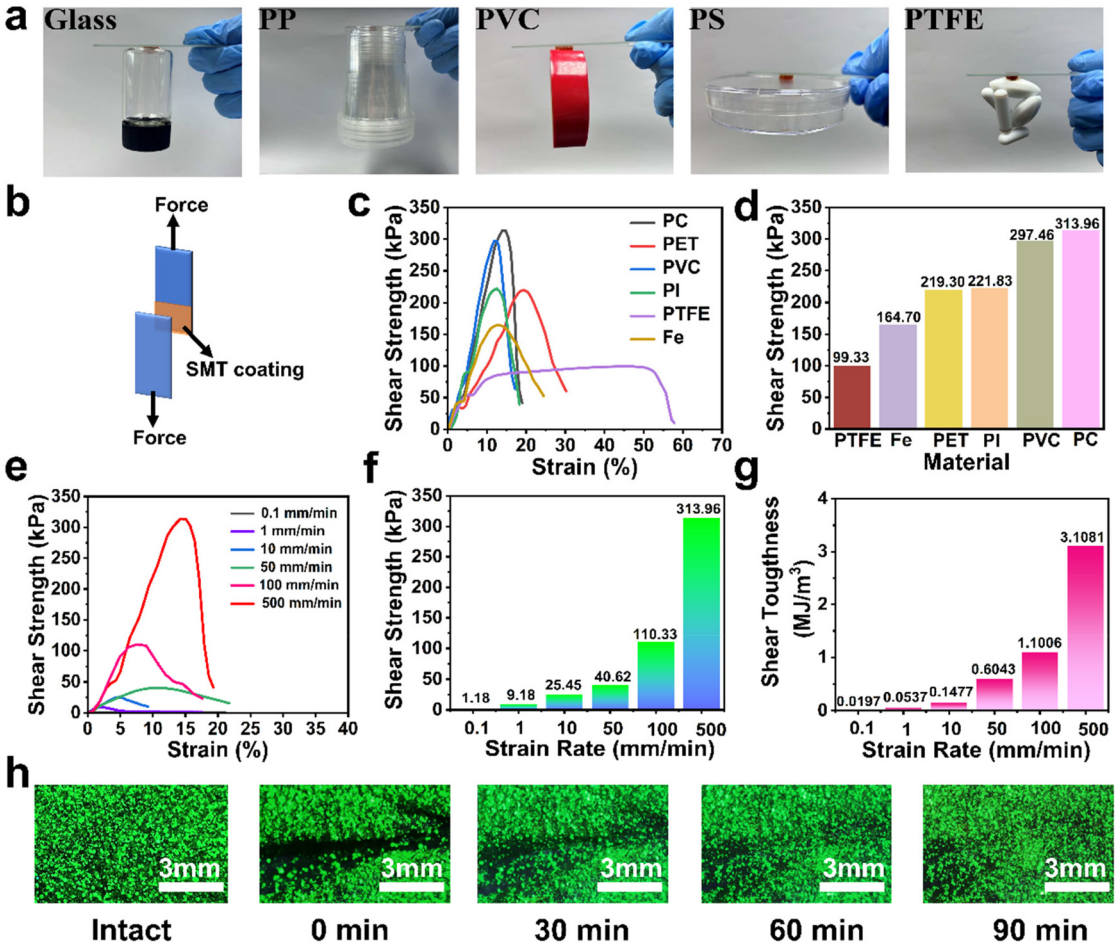

Fig. 3 Mechanical properties of SMT coatings. (a) SMT coatings adhering to different materials. (b) Schematic diagram of SMT coatings in shear experiments. (c) Stress–strain curves of SMT coatings on materials of different shear strength. (d) Shear strength of SMT coatings on different materials. (e) Stress–strain curve of the shear strength of SMT coating bonded to PC material at different strain rates. (f) The maximum shear strength of PC at different strain rates. (g) The fracture energy of PC at different strain rates. (h) The self-healing process of a surface crack of an SMT coating at 35 °C.

Published on 02 noviembre 2024. Downloaded on 05/02/2026 6:04:43.

strength in Fig. 3e. The shear toughness for tensile speeds of 500, 100, 50, 10, 1, and 0.1 mm min^{-1} were 3.1081, 1.1006, 0.6043, 0.1477, 0.0537, and 0.0197 MJ m^{-3}, respectively. The results show that the shear toughness of SMT coatings increases with an increase in tensile speed. To verify the effect of cross-linking density on SMT coatings, different amounts of tannic acid (which primarily provide hydrogen bond interactions) were utilized. As shown in Fig. S5,† with an increase in tannic acid the mechanical properties increase at first and then decrease, and the highest shear strength was observed in the samples with a tannic acid content of 0.5 g. The effect of strain rate strengthening exhibited by the coatings is more beneficial for materials to withstand high-speed loading conditions such as impacts, improving the protective properties of the metal substrate material. Excellent self-healing ability is massively important for actual applications of a coating. To verify the self-healing ability of our SMT coating, the surface of the sample was scratched with a surgical blade, and the samples were self-healed at 35 °C. Since SMT coating is non-transparent, continuous observation with an electron optical microscope showed that samples with scratches can recover to their original state under 35 °C and the scar at the damage site almost completely disappears, and the whole process lasts for 90 min (Fig. 3h and Movie S1†). The healed coating was subjected to a lap shear test. The lap shear test results show the excellent self-healing performance of the SMT coating, which possesses a relatively high shear strength of 255.23 kPa after the healing process (Fig. S6†), and the shear strength was maintained above 81.29% after self-healing. The self-healing ability of the SMT coating comes through the polyphenol–metal coordination bond and a large number of hydrogen bonds, where the reversible dynamic non-covalent bonds are restructured to restore the damaged structure and state.[42,43,52] The achievement of self-healing also relies on the segmental motion of macromolecules, which provides possibilities for the sufficient dissociation and reconstruction of H-bonds. Differential scanning calorimetry (DSC) was carried out (Fig. S7†) and the glass transition temperature (T_g) of SMT coating is −1.1 °C, which indicates that at room temperature the chain segments possess the desired motion ability to support the self-healing behaviors.

Application of photoluminescence (PL) behaviour in crack detection and analysis

The luminescence performance of SMT coating was investigated. Fig. 4a shows the PL intensity and afterglow attenuation behaviour. The $SrAl_2O_4$:Eu^{2+},Dy^{3+} powder and SMT coating were evenly mixed and excited by a Xe lamp for 20 min. The overall afterglow decay behaviours with time show a quick downward trend within 60 min and then level off until 90 min.

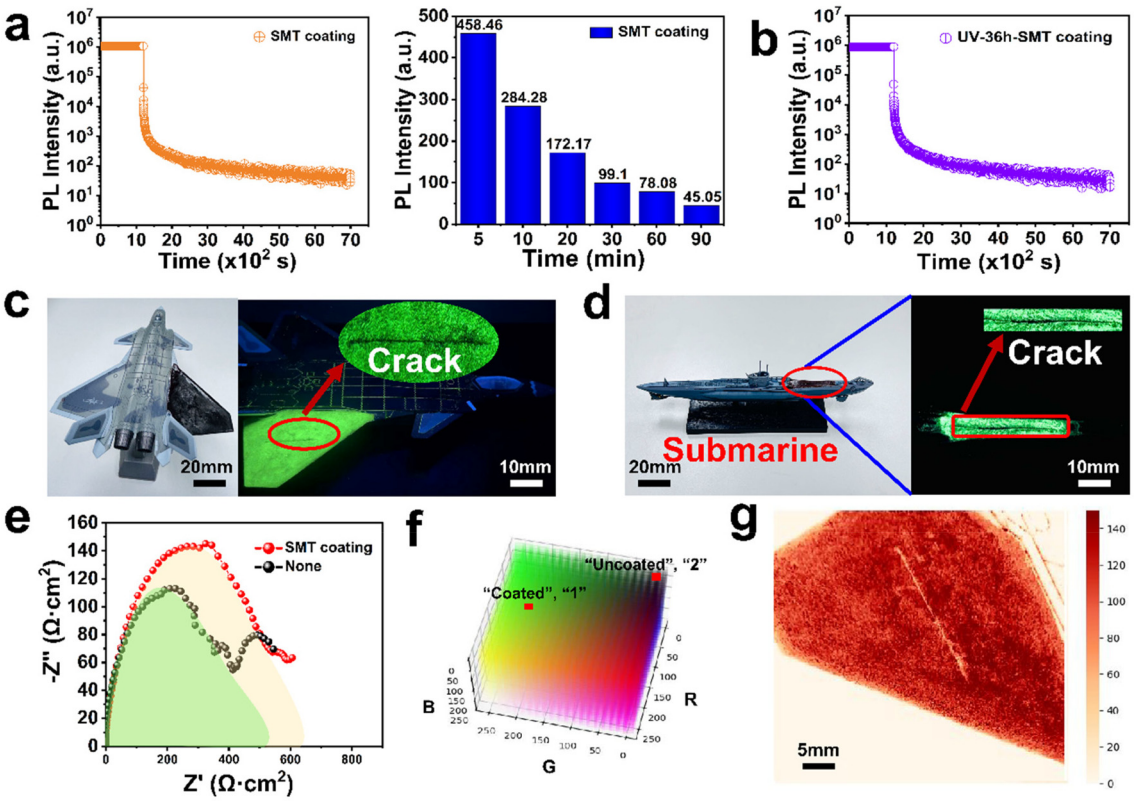

Fig. 4 (a) Photoluminescence (PL) intensity with time for SMT coating. (b) PL intensity with time for UV-36 h SMT coating. (c and d) Demonstration images of the SMT coating on a model of an airplane and a submarine alloy model: (c) shows the Chinese J-20 aircraft model; (d) shows the submarine alloy model. (e) Nyquist plots of pure carbon steel (none) and SMT coating coated carbon steel electrodes immersed in 3.0 wt% NaCl solution. (f) 3D CIE RGB chromaticity diagram of SMT coating. (g) Heat map generated based on the green intensity of the aircraft model.

 This journal is © The Royal Society of Chemistry 2024

Published on 02 noviembre 2024. Downloaded on 05/02/2026 6:04:43.

Fig. 4b shows the afterglow decay curve after 36 h of cumulative UV lamp irradiation. Similarly, the afterglow decay behaviours are similar to that of SMT, with small fluctuations in amplitude. After 180 h of cumulative UV irradiation, the attenuation rates of PL intensity in different periods were measured. Fig. S8† shows a comparison of the attenuation rates of SMT coating, UV-36 h, and UV-180 h SMT coating. In the time periods of 5–10 and 10–20 min, the attenuation rates gradually increase, but the range of fluctuation is small. However, in the following time periods, their afterglow decay rates have changed to different extents. In order to explore the relationship between the doping ratio of powder and polymer, four groups of coatings containing varying amounts of modified $SrAl_2O_4$:Eu^{2+},Dy^{3+} powder were placed under a UV lamp (Fig. S8†). When the doping ratio reached 40%, the luminescent intensity remained almost constant with increasing doping ratio. After cumulative exposure for 180 h, the samples still retained a brightness that was recognizable by the naked eye in the dark (Fig. S10†). This indicates that the SMT coating maintained its luminescent properties under prolonged UV irradiation, allowing for visibility in low-light or dark conditions. Furthermore, under the ultraviolet lamp, the state and luminance of the SMT coating were recorded with the camera every 36 h (Fig. S11†). It can be concluded from the observations that there is no significant difference in the luminescence brightness of the coating as the cumulative exposure time of the ultraviolet lamp increases. This is explained by the SMT coating possessing excellent UV weathering resistance, which is attributed to the polyphenol structure with tannic acid in the SMT system.[53] The SMT coating was applied to the wing of a model aircraft (Fig. 4c) and the surface of a model submarine (Fig. 4d), and then the models were placed under a UV lamp (365 nm). Simultaneously, cracks were artificially induced in the coating using a surgical blade. It can clearly be observed that the brightness of the cracks is significantly weaker than that of other areas. Organic coating on metal substrate is an effective means to delay the corrosion rate of the metal substrate by preventing the metal substrate from coming into contact with a corrosive medium. EIS measurements were conducted to characterize the anticorrosion performance of SMT-coated sheet steel. The measurements were performed under alternating current signals with frequencies from 10^5 to 10^{-1} Hz. Fig. 4e shows the EIS results (Nyquist Plot) for SMT-coated sheet steel. The coatings were coated on sheet steel, and then the sheet steel was immersed in 3.0 wt% NaCl. In general, a wider diameter of the semicircle in the Nyquist plot indicates better corrosion resistance, whereas a smaller semicircle diameter and impedance suggest a higher corrosion rate.[54] From the Nyquist plots in Fig. 4e, the SMT coated steel has the largest semicircle diameter and impedance value. The impedance of SMT-coated sheet steel is 145 Ω cm^2, while that of the pure steel sheet is 113 Ω cm^2, and its impedance value is increased by 28.31%, indicating it shows anticorrosion performance.

According to the theory of three primary colors, the luminescence could be quantitatively analyzed by the intensity of three basic colors: red (R), green (G), and blue (B). From the photographs in Fig. 4c, the RGB values of the luminescent area could be read as 97, 230 and 79, respectively, while the values of the background are 1, 4, and 21. Here, according to our developed 3D CIE RGB chromaticity diagram (Fig. 4f), it can easily be found that the intensity of the green color is the key difference in the color distributions. By extracting the intensity of green in the image pixel by pixel and constructing a matrix to generate a heat map, as shown in Fig. 4g, the distribution of green luminescence can be presented in real time (Movie S2†), which is expected to greatly benefit the identification of crack areas. Moreover, by searching the boundaries of intensity distribution pixel by pixel, the cracks could be presented more intuitively, as shown in the right-hand part, and the theoretical analysis accuracy could approach pixel level (Fig. S12†).

SMT coating degradation and $SrAl_2O_4$:Eu^{2+},Dy^{3+} powder recycling

Based on the concepts of sustainable development and environmental protection, the biodegradability of this biosource coating was further studied. Fig. 5a shows the degradation of the SMT coating in bamboo powder with increasing burial time. Different colored arrows were used to represent different components, where the red circle, blue circle, green circle, black circle, and yellow circle represent SMT coating, bamboo powder, $SrAl_2O_4$:Eu^{2+},Dy^{3+} powder, coating degradation, and bacteria respectively. SMT coatings can be degraded in bamboo powder, and the degree of degradation increases with the increase in number of days buried. After 5 days of burial, the SMT coating cannot be observed by the naked eye. The SMT coating was exposed to an open environment (Hainan province, a tropical area of China) for six months without degradation. As shown in Fig. S13,† after six months there is no visible difference compared to newly fabricated samples, and the corresponding FTIR spectra as supplied in Fig. S14† also remain consistent. Finally, bacterial colonies were also observed in the degradation chain (Fig. S15†). The SMT coating could only be degraded under anaerobic composting conditions with the help of specific kinds of microorganism.[55,56] Fig. 5b and c show the recycling process of the degraded powder. A mixture of $SrAl_2O_4$:Eu^{2+}, Dy^{3+} powder and bamboo powder was placed in a container, and further degradation of the bamboo powder was achieved by cellulase. The modified $SrAl_2O_4$:Eu^{2+},Dy^{3+} powder can be recycled. Upon subjecting the recycled powder to FTIR analysis (Fig. S16†), the characteristic peak at 1090 cm^{-1} belonging to the Si–O bond is evident, confirming the retention of the silica layer on the powder surface. Fig. 5d shows a comparison of PL intensity between recycled $SrAl_2O_4$:Eu^{2+},Dy^{3+} powder and SMT coating at different time points: the intensity of the afterglow decreased little at these six time points of 5, 10, 20, 30, 60, and 90 min and the PL intensity of the recycled powder was maintained at 95.19% at the time point of 5 min. The attenuation curve of the recycled $SrAl_2O_4$:Eu^{2+},Dy^{3+} powder was compared with that of the modified $SrAl_2O_4$:Eu^{2+},Dy^{3+} powder (Fig. S17†).

Published on 02 noviembre 2024. Downloaded on 05/02/2026 6:04:43.

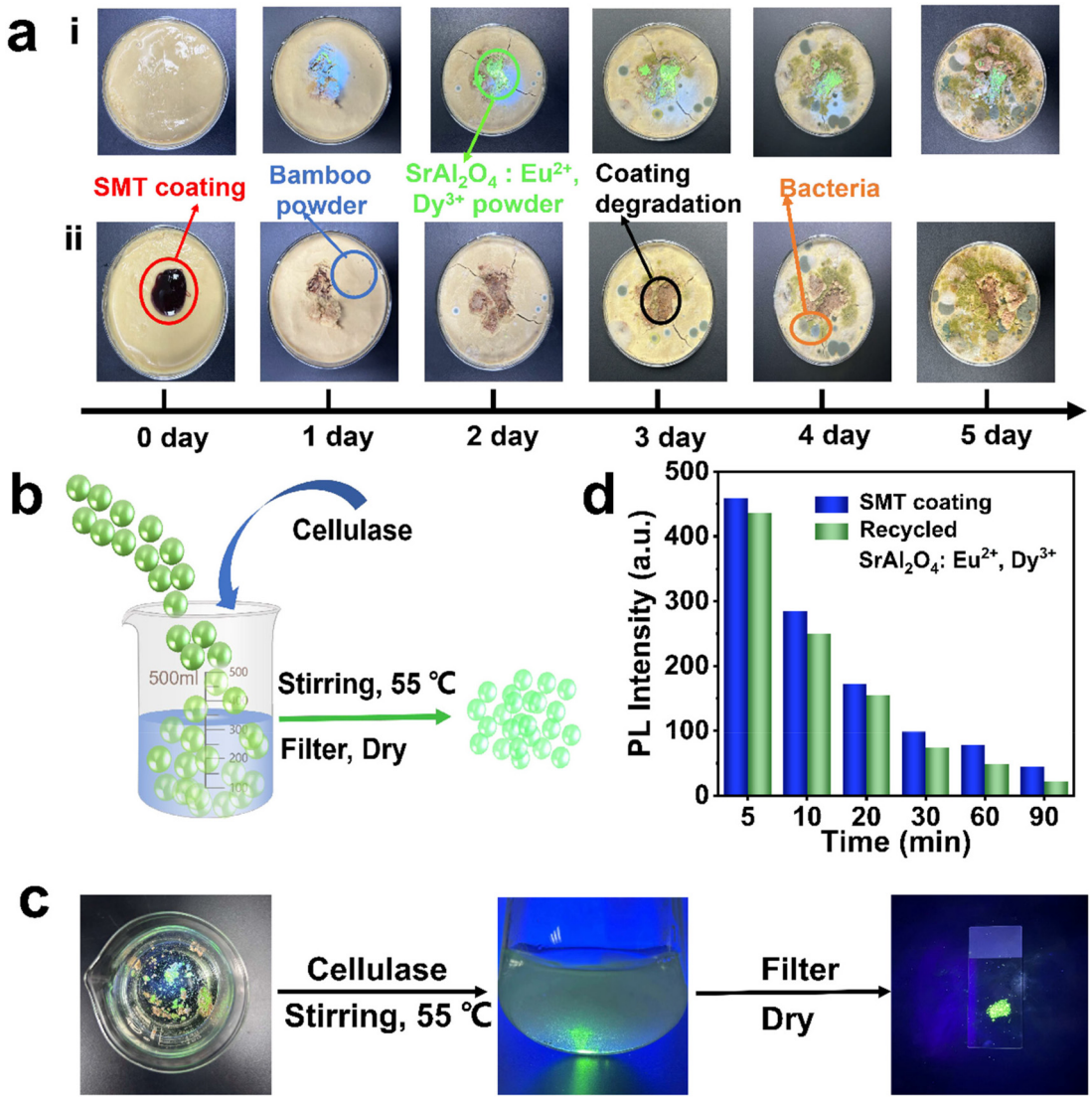

Fig. 5 (a) Degradation process of SMT coating buried in bamboo powder. (i) represents the image of the SMT coating degradation process under ultraviolet flashlight irradiation, and (ii) represents the image of the SMT coating degradation process under sunlight. Different colored arrows are used to represent different components. (b) Schematic of the $SrAl_2O_4$:Eu^{2+},Dy^{3+} powder recycling process. (c) The $SrAl_2O_4$:Eu^{2+},Dy^{3+} powder recycling process. (d) PL intensity comparison between recycled $SrAl_2O_4$:Eu^{2+},Dy^{3+} powder and SMT coating. After an Xe lamp is used as an excitation source and continuously excited for 20 min, the PL intensity for different time points is collected.

In the periods of 5–10, 20–30, and 60–90 min after the removal of the excitation source, the attenuation degree of the PL intensity of the recycled $SrAl_2O_4$:Eu^{2+},Dy^{3+} powder surpassed that of the modified $SrAl_2O_4$:Eu^{2+},Dy^{3+} powder by 5.36%, 20.72%, and 21.91%, respectively. However, during the periods of 10–20 and 30–60 min, the attenuation rate of the recycled $SrAl_2O_4$:Eu^{2+}, Dy^{3+} powder was found to be lower than that of the modified $SrAl_2O_4$:Eu^{2+},Dy^{3+} powder, by 2.94% and 13.32%, respectively. This indicates that the luminescence effect of the recycled powder is slightly decreased. Compared with traditional coatings, SMT coatings exhibit remarkable biodegradability, allowing for faster decomposition after disposal, thus significantly reducing pollution to the ecological environment. Furthermore, the recycling and reuse of $SrAl_2O_4$:Eu^{2+},Dy^{3+} powder comply with the requirements of the circular economy, embodying the green, circular, and low-carbon development philosophy.

Conclusions

An environmental-friendly and bio-degradable intelligent coating based on bio-sourced polymers and modified long afterglow powders has been presented. The dynamic hydrogen bonding network endows the coating with desirable adhesive performances (313.96 kPa) and self-healing ability (self-healing efficiency 81.29%). By compositing with SiO_2-modified $SrAl_2O_4$:Eu^{2+},Dy^{3+} powder and developing a quantitative luminescence-analysing tool, an intelligent coating with long

 This journal is © The Royal Society of Chemistry 2024

afterglow ability is able to monitor small cracks by visualization. Moreover, the obtained bio-sourced composites could be degraded under anaerobic composting conditions within 5 days, and after degradation the long afterglow powders could be separated and recycled with almost consistent performance (luminescent intensity remains 95.19%) compared to the original powders. This work not only provides a valuable example for bio-sourced intelligent coatings, but also open up new opportunities for the utilization of bio-sourced materials.

Data availability

All data included in this study are available upon request by contact with the corresponding author.

Conflicts of interest

There are no conflicts to declare.

Acknowledgements

The authors thank the Innovational Fund for Scientific and Technological Personnel of Hainan Province (KJRC2023C09), Start-up Scientific Research Foundation from Hainan University (KYQD(ZR)22174), Opening Project of Guangxi Key Laboratory of Calcium Carbonate Resources Comprehensive Utilization (HZXYKFKT202301).

References

1 T. Yimyai, D. Crespy and M. Rohwerder, *Adv. Mater.*, 2023, **35**, 2300101.
2 D. Zang, R. Zhu, W. Zhang, X. Yu, L. Lin, X. Guo, M. Liu and L. Jiang, *Adv. Funct. Mater.*, 2017, **27**, 1605446.
3 Y. Ye, Z. Liu, W. Liu, D. Zhang, H. Zhao, L. Wang and X. Li, *Chem. Eng. J.*, 2018, **348**, 940–951.
4 C. Liu, H. Zhao, P. Hou, B. Qian, X. Wang, C. Guo and L. Wang, *ACS Appl. Mater. Interfaces*, 2018, **10**, 36229–36239.
5 C. Zhu, Y. Fu, C. Liu, Y. Liu, L. Hu, J. Liu, I. Bello, H. Li, N. Liu, S. Guo, H. Huang, Y. Lifshitz, S.-T. Lee and Z. Kang, *Adv. Mater.*, 2017, **29**, 1701399.
6 B. Zhang, G. Yang, W. Xu, J. Duan and B. Hou, *J. Mater. Sci. Technol.*, 2024, **184**, 256–268.
7 Y. Bai, T. Guo, J. Wang, J. Gao, K. Gao and X. Pang, *Acta Mater.*, 2021, **217**, 117179.
8 W. Gu, W. Li, Y. Zhang, Y. Xia, Q. Wang, W. Wang, P. Liu, X. Yu, H. He, C. Liang, Y. Ban, C. Mi, S. Yang, W. Liu, M. Cui, X. Deng, Z. Wang and Y. Zhang, *Nat. Commun.*, 2023, **14**, 5953.
9 X. Qi, D. Zhang, Z. Ma, W. Cao, Y. Hou, J. Zhu, Y. Gan and M. Yang, *ACS Nano*, 2018, **12**, 1062–1073.
10 J. Liu, F. Recupido, G. C. Lama, M. Oliviero, L. Verdolotti and M. Lavorgna, *Collagen Leather*, 2023, **5**, 8.
11 S. Gazzotti, M. Hakkarainen, C. A. Pagnacco, M. Manenti, A. Silvani, H. Farina, L. Arnaboldi and M. A. Ortenzi, *Polym. Chem.*, 2024, **15**, 2081–2093.
12 S. L. Wright and F. J. Kelly, *Environ. Sci. Technol.*, 2017, **51**, 6634–6647.
13 Y. W. Chek and D. T.-C. Ang, *Prog. Org. Coat.*, 2024, **188**, 108190.
14 Z. Song, F. Gao, W. Zhang, J. Zhong, Y. Wu, Y. Liu, X. Gao and L. Shen, *Prog. Org. Coat.*, 2023, **183**, 107816.
15 P. Feng, H. Wang, S. Gan, B. Liao and L. Niu, *Small*, 2024, **n/a**, 2312085.
16 S. Tang, J. Li, R. Wang, J. Zhang, Y. Lu, G.-H. Hu, Z. Wang and L. Zhang, *SusMat*, 2022, **2**, 2–33.
17 F. Vidal, E. R. van der Marel, R. W. F. Kerr, C. McElroy, N. Schroeder, C. Mitchell, G. Rosetto, T. T. D. Chen, R. M. Bailey, C. Hepburn, C. Redgwell and C. K. Williams, *Nature*, 2024, **626**, 45–57.
18 N. Zhang, C. Gao, L. Meng and X. Tang, *Carbohydr. Polym.*, 2023, **319**, 121224.
19 J. Ho, B. Mudraboyina, C. Spence-Elder, R. Resendes, M. F. Cunningham and P. G. Jessop, *Green Chem.*, 2018, **20**, 1899–1905.
20 G. Yang, Z. Gong, X. Luo, L. Chen and L. Shuai, *Nature*, 2023, **621**, 511–515.
21 P. Sun, S. Mei, J.-F. Xu and X. Zhang, *Adv. Sci.*, 2022, **9**, 2203182.
22 C. R. Westerman, B. C. McGill and J. J. Wilker, *Nature*, 2023, **621**, 306–311.
23 X. Fang, N. Tian, W. Hu, Y. Qing, H. Wang, X. Gao, Y. Qin and J. Sun, *Adv. Funct. Mater.*, 2022, **32**, 2208623.
24 S. Ammar, A. W. M. Iling, K. Ramesh and S. Ramesh, *Prog. Org. Coat.*, 2020, **140**, 105523.
25 X.-Y. Jian, Y. He, Y.-D. Li, M. Wang and J.-B. Zeng, *Chem. Eng. J.*, 2017, **326**, 875–885.
26 H. Tong, H. Li, H. Li, Cidanpuchi, F. Wang and W. Liu, *Inorg. Chem.*, 2021, **60**, 15049–15054.
27 X. Chen, G. Wang, M. Wu, J. Liu, Z. Liu, X. Wang, Y. Zou and K. Zhang, *Polym. Chem.*, 2022, **13**, 4641–4649.
28 Z. Huang, B. Chen, B. Ren, D. Tu, Z. Wang, C. Wang, Y. Zheng, X. Li, D. Wang, Z. Ren, S. Qu, Z. Chen, C. Xu, Y. Fu and D. Peng, *Adv. Sci.*, 2023, **10**, 2204925.
29 X. Yang, G. I. N. Waterhouse, S. Lu and J. Yu, *Chem. Soc. Rev.*, 2023, **52**, 8005–8058.
30 S. Liu, N. Mao, Z. Song and Q. Liu, *ACS Appl. Mater. Interfaces*, 2022, **14**, 1496–1504.
31 Y. Zhou, P. Zhang, Z. Liu, W. Yan, H. Gao, G. Liang and W. Qin, *Adv. Mater.*, 2024, **n/a**, 2312439.
32 J. Liu, G. C. Lama, F. Recupido, C. Santillo, G. Gentile, G. G. Buonocore, L. Verdolotti, X. Zhang and M. Lavorgna, *Compos. Sci. Technol.*, 2023, **236**, 109993.
33 J. Liu, X. Li, X. Yang and X. Zhang, *Adv. Intell. Syst.*, 2021, **3**, 2000183.
34 L. Zhang, D. Wang, L. Xu and A. Zhang, *Polym. Chem.*, 2021, **12**, 660–669.
35 S. Y. Zheng, J. Zhou, S. Wang, Y.-J. Wang, S. Liu, G. Du, D. Zhang, J. Fu, J. Lin, Z. L. Wu, Q. Zheng and J. Yang, *Adv. Funct. Mater.*, 2022, **32**, 2205597.

Published on 02 noviembre 2024. Downloaded on 05/02/2026 6:04:43.

Published on 02 noviembre 2024. Downloaded on 05/02/2026 6:04:43.

36 Y. Zhuang and R.-J. Xie, *Adv. Mater.*, 2021, **33**, 2005925.
37 S. Timilsina, R. Bashnet, S. H. Kim, K. H. Lee and J. S. Kim, *Int. J. Fatigue*, 2017, **101**, 75–79.
38 J. Liu, F. Zhao, Q. Tao, J. Cao, Y. Yu and X. Zhang, *Mater. Horiz.*, 2019, **6**, 1892–1898.
39 H. Wu, J. Li, W. Zhang, T. Chen, F. Liu and E.-H. Han, *Chem. Eng. J.*, 2022, **437**, 135405.
40 J. Chen, Z. Wang, B. Yao, Y. Geng, C. Wang, J. Xu, T. Chen, J. Jing and J. Fu, *Adv. Mater.*, 2024, **36**, 2401178.
41 J. Cao, C. Zhou, G. Su, X. Zhang, T. Zhou, Z. Zhou and Y. Yang, *Adv. Mater.*, 2019, **31**, 1900042.
42 C.-H. Li and J.-L. Zuo, *Adv. Mater.*, 2020, **32**, 1903762.
43 Y. Guo, X. An and X. Qian, *ACS Appl. Mater. Interfaces*, 2023, **15**, 19362–19373.
44 T. Qi, H. Xia, Z. Zhang, S. Kong, W. Peng, Q. Zhao and Z. Huang, *Solid State Sci.*, 2017, **65**, 88–94.
45 Y. Chen, F. Tian, J. Yao, L. Li, Y. Cui, H. Yang, Z. Chen, G. Sun, P. S. Shuttleworth and H. Yue, *ACS Appl. Polym. Mater.*, 2024, **6**, 6469–6481.
46 H. Long, L. Hu, F. Yang, Q. Cai, Z. Zhong, S. Zhang, L. Guan, D. Xiao, W. Zheng, W. Zhou, Y. Wei, K. Frank and X. Dong, *Composites, Part B*, 2022, **239**, 109968.
47 K.-X. Hou, P.-C. Zhao, L. Duan, M. Fan, P. Zheng and C.-H. Li, *Adv. Funct. Mater.*, 2023, **33**, 2306886.
48 X. Huang, X. Yang, H. Liu, S. Shang, Z. Cai and K. Wu, *Ind. Crops Prod.*, 2019, **139**, 111540.
49 X. Wang, X. Huang, Z. Ji, H. Sheng and H. Liu, *ACS Sustainable Chem. Eng.*, 2024, **12**, 7147–7157.
50 Y. Ma, Y. Hu, Z. Kou, M. Zhang, L. Hu, S. Li, Q. Huang, P. Jia, Y. Zhou and F. Chu, *Ind. Crops Prod.*, 2024, **209**, 118048.
51 Z. Xu, L. Chen, L. Lu, R. Du, W. Ma, Y. Cai, X. An, H. Wu, Q. Luo, Q. Xu, Q. Zhang and X. Jia, *Adv. Funct. Mater.*, 2021, **31**, 2006432.
52 H. Zhang, B. Wang, J. Han, X. Shen, Q. Sun, Y. An, R. Luo and Y. Wang, *Chem. Eng. J.*, 2024, **482**, 149020.
53 R. Wang, X. Wang, Y. Zhan, Z. Xu, Z. Xu, X. Feng, S. Li and H. Xu, *ACS Appl. Mater. Interfaces*, 2019, **11**, 37502–37512.
54 J. Tong, W. Pan, J. Ma, J. Luo and R. Liu, *Prog. Org. Coat.*, 2023, **175**, 107366.
55 M. S. Kim, H. Chang, L. Zheng, Q. Yan, B. F. Pfleger, J. Klier, K. Nelson, E. L. W. Majumder and G. W. Huber, *Chem. Rev.*, 2023, **123**, 9915–9939.
56 M. Guicherd, M. Ben Khaled, M. Guéroult, J. Nomme, M. Dalibey, F. Grimaud, P. Alvarez, E. Kamionka, S. Gavalda, M. Noël, M. Vuillemin, E. Amillastre, D. Labourdette, G. Cioci, V. Tournier, V. Kitpreechavanich, P. Dubois, I. André, S. Duquesne and A. Marty, *Nature*, 2024, **631**, 884–890.

This journal is © The Royal Society of Chemistry 2024